JOURNAL OF Materials CHEMISTRY

XRD, TEM and ^{29}Si MAS NMR study of sol–gel ZnO–SiO_2 nanocomposites

Carla Cannas, Mariano Casu,* Adolfo Lai, Anna Musinu and Giorgio Piccaluga

Dipartimento di Scienze Chimiche, Universita' di Cagliari, Via Ospedale 72, I-09124 Cagliari, Italy. E-mail: mariano@mvcch3.unica.it

Received 5th February 1999, Accepted 18th May 1999

X-Ray amorphous ZnO nanoparticles homogeneously dispersed in a silica matrix were evidenced in ZnO–SiO_2 nanocomposites obtained by a sol–gel method and heated to 700 °C. TEM observations indicated that the particle size slowly increases with temperature and zinc oxide content, reaching an upper limit of 12 nm. Through a comparison of the ^{29}Si MAS NMR data of the nanocomposites and silica samples, obtained by the same preparation method, it was possible to observe that reaction occurs between ZnO and silica on heating, which causes a depolymerization of the host matrix with the formation of low condensation groups. This result is discussed in terms of interactions between nanoparticles and the silica matrix at the nanoparticle/matrix interface. A further increase in temperature (900 °C) results in the formation of the β-Zn_2SiO_4 crystalline phase.

Introduction

Nanocomposite materials are of great interest because of their potential use in a variety of fields, such as catalysis, optics, magnetism and electronics.[1] The properties of a nanocomposite are strongly dependent on its microstructure, not only in terms of dispersion, size distribution of metal or metal oxide nanoparticles and features of the matrix support, but also as a function of possible interactions that might take place between nanoparticles and the matrix. For M (or MO)/SiO_2 materials, such interactions can be related to the adopted preparation method,[2–4] which range from the formation of 'true' compounds (phyllosilicates) in systems obtained by impregnation to the arrangement of electrostatic interactions and/or hydrogen bonds among silanol groups and water molecules close to the nanoparticles in composites obtained by a sol–gel route.[5]

We recently investigated the physical and structural properties of some Fe_2O_3–silica nanocomposites prepared by a simple sol–gel method,[6,7] which led to metal oxide nanoparticles being homogeneously dispersed within an amorphous silica matrix. The influence of the nanoparticles on the silica support has been studied by IR and NMR spectroscopies,[8] which indicate that Fe_2O_3 nanoparticles interact with the silanol groups at the surface of the cavities in which they form.

In the present work, the study has been extended to the ZnO–SiO_2 system. ZnO-based nanocomposites are promising materials in ceramics technology for application as varistors, sensor elements, photoconductors in electrophotography, *etc.* In particular, varistors used in high voltage applications require a relatively small grain size (a few μm) in order to keep the varistor volume low, while the overall properties of varistors are greatly improved by a further reduction of the size of the particles to the nm range.[9,10] Some methods for the preparation of ZnO nanopowders aimed at studying the effects of process variables on the microstructure and on the growth of particles have been proposed in the literature.[10–12] Some authors[11–13] have proposed dispersion of zinc oxide nanoparticles over ceramic matrices in order to avoid the tendency of nanopowders to aggregate and control the nanoparticle size distribution. In particular, Khouchaf *et al.*[13] report a structural characterization of a fine dispersion of zinc oxide particles within the nanopores of a zeolite. The atomic structure of the particles and their interaction with the microporous framework was investigated by EXAFS spectroscopy,[13] which showed the presence of bonds between small clusters of zinc cations adsorbed on the sodalite network and the matrix itself. The present study focuses on the structural properties of ZnO–SiO_2 nanocomposites, obtained by the sol–gel method, with particular emphasis on the nanoparticle matrix interface. This work may also lead to an easy, effective preparation method for these materials.

ZnO–SiO_2 nanocomposites containing 17 and 34 wt% ZnO were obtained by the sol–gel method previously used for the preparation of Fe_2O_3–SiO_2 nanocomposites. The structural evolution upon heating of the amorphous and crystalline phases and the particle size distribution were investigated by XRD and TEM; the structural modifications of the silica matrix induced by zinc oxide were studied by ^{29}Si MAS NMR and CP MAS NMR.

Experimental

Two ZnO–SiO_2 composites containing 17 and 34 wt% of zinc oxide were prepared by a sol–gel method. An ethanolic solution of tetraethoxysilane (TEOS, Aldrich 98%) was mixed with an aqueous solution of zinc nitrate ($Zn(NO_3)_2{\cdot}6H_2O$, Aldrich 98%), following the procedure described in previous work.[6] The systems with different Zn contents were obtained using aqueous solutions of different zinc nitrate concentrations. After stirring for 1 h, the clear sols were poured into Teflon beakers and allowed to gel in the air. The gels were allowed to dry for *ca.* one week with the temperature allowed to slowly rise to 90 °C. The samples were then powdered and heated to temperatures up to 900 °C, in steps of 100 °C maintaining the temperature at each step for 30 min. The same procedure was used to prepare the silica matrix as a reference sample. Samples are denoted Zn_xY and SiY, where Y indicates the treatment temperature (T_{treat}) and x the wt% of ZnO.

The structural evolution of the samples as a function of T_{treat} and composition was monitored by XRD using a θ–2θ mode conventional diffractometer (Siemens D500) with Mo-Kα radiation; zinc oxide nanoparticles were observed by electron microscopy using a TEM (JEOL 200CX) operating at 200 kV; electron diffraction micrographs were obtained with the selected area diffraction (SAD) mode.

High resolution NMR spectra were collected using a Varian Unity Inova spectrometer with a 9.39 T wide-bore Oxford magnet. The MAS experiments were performed with a probe equipped with 7 mm ZrO_2 rotors at a spinning rate of 6 kHz. The ^{29}Si MAS experiments were run with a recycle time of 500 s, 45° pulse lengths (4.5 ms), a 100 kHz bandwidth and 200

scans in each experiment. The CP MAS NMR spectra were collected with a contact time of 4 ms and a recycle time of 5 s. The ^{29}Si chemical shifts were referenced to tetramethylsilane.

The Q_n distributions were obtained by a non-linear fitting of the NMR spectra to gaussian lineshapes by means of the Origin 4.1 program from Microcal Software.

Results

The spectra of the Zn_{17} and Zn_{34} samples are shown in Fig. 1(a) and (b), respectively. The XRD spectra of the two nanocomposites of different concentrations show a similar evolution as a function of T_{treat}. XRD patterns from Zn_x300 to Zn_x700 do not display any diffraction peaks with only the amorphous pattern of vitreous silica being visible for Zn_x300. Upon further heating the amorphous background undergoes minor changes and two broadened bands, whose intensity slowly rises with zinc oxide concentration and T_{treat}, emerge in the ranges 2θ 15–18 and 27–31°. In agreement with the TEM observations reported below, the bands can be ascribed to the presence of zinc oxide nanoparticles. The samples treated up to $T \leqslant 850$ °C do not exhibit any crystalline phases, while at 900 °C the spectra change abruptly, showing the presence of a sequence of crystalline peaks ascribed to β-Zn_2SiO_4[14] emerging from a residual amorphous pattern. This crystalline component, as expected, is more abundant for the $Zn_{34}900$ sample.

TEM observations show the presence of nanoparticles dispersed within the silica matrix in all the samples treated up to 700 °C. As an example, a bright field micrograph of the $Zn_{17}700$ sample is shown in Fig. 2, showing the nanoparticles homogeneously distributed within the silica support. In agreement with the XRD spectra, dark field observations indicate

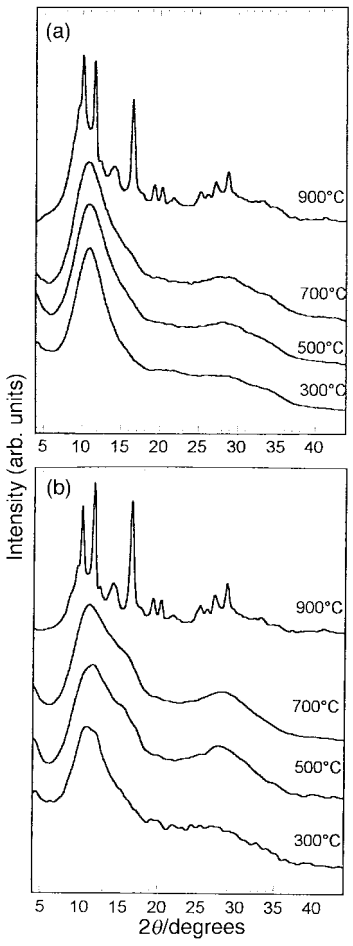

Fig. 1 XRD data of (a) the $Zn_{17}Y$ and (b) the $Zn_{34}Y$ sample.

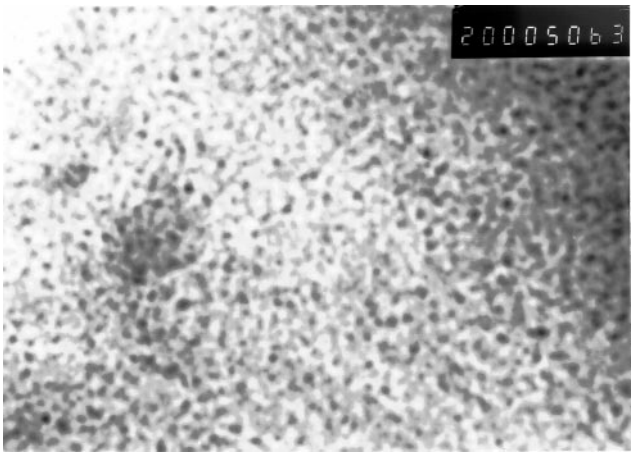

Fig. 2 TEM bright field image of the $Zn_{17}700$ sample (×200 000).

the amorphous character of the majority of the nanoparticles. The particle size increases slightly with zinc oxide content and T_{treat}, from an average value of *ca.* 3–6 nm for $Zn_{17}300$ to an average of *ca.* 8–12 nm for $Zn_{34}700$, while the size distribution becomes less narrow. In the latter case, it was possible to find particles that gave rise to diffraction rings through which they could be identified and a SAD pattern is shown in Fig. 3 which shows a series of rings ascribed to the main reflections of the ZnO zincite phase.[15]

^{29}Si MAS NMR spectra of the $Zn_{17}Y$ and $Zn_{34}Y$ samples and of the corresponding silica matrix samples (SiY) are shown in Fig. 4. The spectra of the silica samples show three partially overlapping signals falling in the range δ −80 to −120. Their assignment to Q_4, Q_3 and Q_2 groups has been made according to the literature[16] (Q_n represents SiO_4 tetrahedra of an amorphous network which forms n bonds with neighbouring tetrahedra). As expected for silica samples obtained by the sol–gel method,[17] an increase in the number of groups with a higher degree of condensation is observed as a function of T_{treat}. The ^{29}Si MAS spectra of the silica samples were simulated and the chemical shifts and linewidths are reported in Table 1.

The spectra of the Zn_{17} and Zn_{34} samples show a more complex behaviour upon heating (Fig. 4). In particular, in addition to the signals ascribed to the Q_4 and Q_3 groups observed for the silica samples, the spectra of nanocomposites treated up to 700 °C show a broadened shoulder at high frequency (δ −60 to −100), thus suggesting the presence of Q_n sites of a lower degree of condensation. In the spectra of both Zn_{17} and Zn_{34} samples at T_{treat} = 900 °C, in addition to low frequency resonances (δ −100 to −110) ascribed to the residual amorphous silica, a high frequency signal consisting

Fig. 3 SAD pattern of the $Zn_{34}700$ sample.

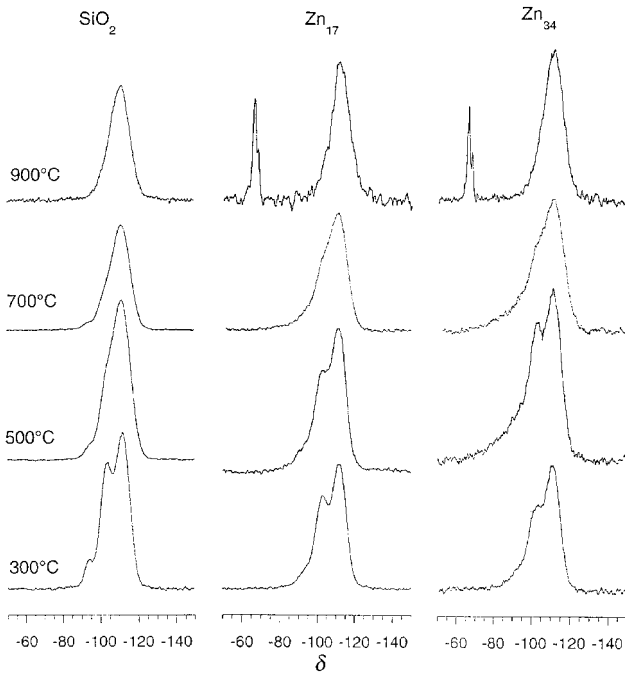

Fig. 4 ^{29}Si MAS NMR spectra of the silica matrix and nanocomposite samples.

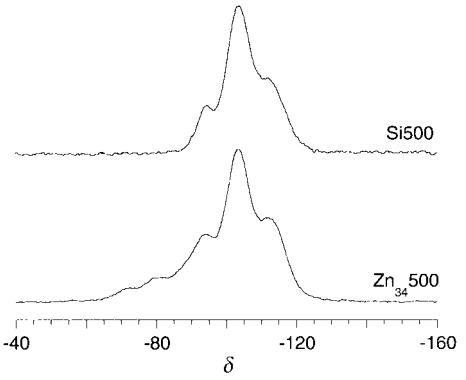

Fig. 5 ^{1}H–^{29}Si CP MAS NMR spectrum of the Zn_{34} and silica matrix samples treated at 500 °C.

of narrow resonances at δ *ca.* −67 is observed. The sharp linewidth of these signals (fwhm < 1.4 ppm) indicates that they pertain to a crystalline component, which can be reasonably ascribed to the β-Zn_2SiO_4 phase revealed by XRD and belong to a Q_0 nesosilicate structure type.[18] The intensity ratios of the amorphous to crystalline signals in the 900 °C spectra for the Zn_{17} and Zn_{34} samples are similar in spite of the different amounts of zinc present. Since the relaxation times of this crystalline component are very long, no information about their relative amount can be extracted.

To single out the resonances in the spectra of the nanocomposites at $T_{treat} \leqslant 700$ °C (Fig. 4), the ^{1}H–^{29}Si CP MAS technique has been used, which allows a selective enhancement of three well resolved signals at high frequencies. As an example, the CP MAS spectrum of the $Zn_{34}500$ sample is shown in Fig. 5, together with the CP MAS spectrum of the Si500 sample. In the spectrum of the nanocomposite, in addition to the Q_4, Q_3 and Q_2 signals for the silica sample, two new signals at high frequency (δ −80 and −70) are observed which can be assigned to Q_1 and Q_0 groups, respectively.[18]

The linewidth of the signals, obtained from the deconvolution of the CP MAS spectra of the Si500 sample, becomes narrower on going from Q_4 (10.5 ppm) to Q_2 (7.4 ppm), in agreement with previous results.[19] In the case of the $Zn_{34}500$ sample, however, the outcome of the fitting procedure of the CP MAS spectrum indicates a larger linewidth for Q_2 (11.8 ppm) than for Q_4 groups (9.7 ppm).

In an attempt to quantify the relative amount of the most abundant species (Q_4, Q_3) as a function of T_{treat}, the ^{29}Si MAS spectra of all Zn_{17} and Zn_{34} nanocomposites were simulated with a maximum of five gaussians, using as constraints the chemical shifts and linewidths obtained by fitting of the ^{1}H–^{29}Si CP MAS spectra; only the amorphous low frequency region was simulated in the spectra at $T_{treat} = 900$ °C.

The trend of Q_4% and Q_3% as a function of T_{treat} is schematically represented in Fig. 6, where the results of each Zn_{17} and Zn_{34} sample are compared with those of the silica matrix, while the outcomes of the fitting procedure are reported in Table 1. For the two nanocomposites treated at 500 and 700 °C, an increase in Q_3 and a strong enhancement of low condensation (Q_{lc}) groups, reported in Table 1 as the sum of Q_2, Q_1 and Q_0, at the expense of the Q_4 groups is observed. Q_{lc} groups are mainly composed by Q_2, and low percentages of Q_1 and Q_0 species, as expected from the observation of the spectra reported in Fig. 4 and 5.

Table 1 Chemical shifts (δ), full width at half maximum [fwhm (ppm)] and percentage of Q_n components (Q%) for SiO_2, SiO_2–ZnO (17%) and SiO_2–ZnO (34%) treated at 300, 500, 700 and 900 °C obtained by deconvolution of MAS spectra

	Si			Zn_{17}			Zn_{34}		
	δ	fwhm	Q%[a]	δ	fwhm	Q%[a]	δ	fwhm	Q%[a]
300 °C									
Q_4	−111.7	8.6	56	−111.5	9.1	57	−111.2	9.1	57
Q_3	−102.8	8.0	38	−101.9	7.9	35	−102.0	8.0	30
Q_2	−93.6	5.8	6						
Q_{lc}						8			13
500 °C									
Q_4	−111.5	10.5	73	−111.2	9.4	58	−111.1	9.8	49
Q_3	−102.0	8.0	23	−101.7	7.9	28	−101.6	8.2	30
Q_2	−93.3	7.4	3						
Q_{lc}						13			23
700 °C									
Q_4	−111.3	10.6	80	−110.6	11.1	66	−110.7	10.5	61
Q_3	−102.3	8.4	17	−101.7	7.9	21	−102.0	9.1	22
Q_2	−93.8	7.7	3						
Q_{lc}						13			17
900 °C									
Q_4	−111.6	11.3	85	−111.3	10.6	83	−111.3	10.7	84
Q_3	−103.0	10.9	15	−103.6	10.1	17	−101.5	10.4	16

[a]Accuracy 3–6%.

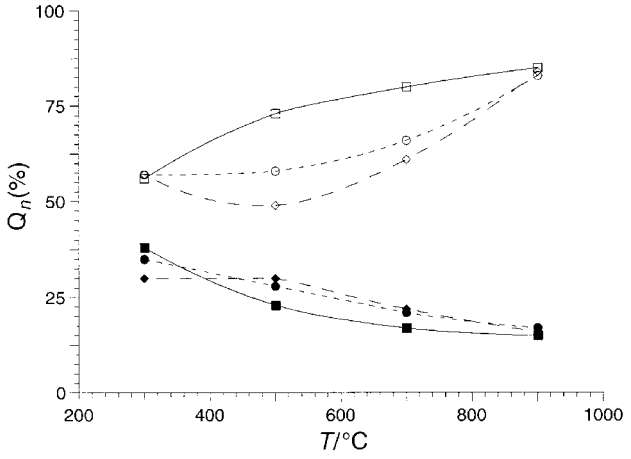

Fig. 6 Relative amount of Q_n species as a function of the treatment temperature. Q_4 (open symbols), Q_3 (full symbols); silica matrix (squares), $Zn_{17}Y$ (circles), $Zn_{34}Y$ (diamonds).

Discussion and conclusion

The sol–gel preparation route reported here has been successful in obtaining $ZnO–SiO_2$ nanocomposites. XRD and TEM investigations show that in the range 300–700 °C, the ZnO nanoparticles, which are mostly amorphous, are homogeneously dispersed within the amorphous silica matrix. The analysis of the structural evolution of these systems indicates that nanoparticle size slowly increases with T_{treat} (up to 700 °C) and ZnO content. At the highest calcination temperature (900 °C), the systems abruptly evolve towards the formation of the β-Zn_2SiO_4 crystalline phase. This transition temperature is significantly higher than that of the corresponding β-Zn_2SiO_4 bulk phase reported in the literature (730 °C),[20] and indicates that the silica matrix plays an important role in stabilising zinc oxide nanoparticles.

Comparison of the ^{29}Si MAS NMR spectra of the nanocomposites with the corresponding spectra of the silica matrix, indicates that the nature and distribution of the Q_n sites are significantly affected by the presence of nanoparticles as a function of temperature and ZnO content. The results indicate a drastic reduction of the percentage of the Q_4 groups in the range 500–700 °C, particularly for the Zn_{34} samples, while the proportion of Q_{lc} groups is higher. Such groups grow at the expense of the Q_4 groups, which are known to increase as a function of temperature due to silica polymerization. Previous ^{29}Si MAS studies on silicate systems[21,22] showed that low condensation groups are present at the matrix surface. Therefore, the observed results suggest that nanoparticles affect the sites that are more exposed at the interface. At first sight, this seems to indicate that the nanoparticles formed in cavities of the matrix act as an obstacle towards spontaneous silica polimerization.

Moreover, important interactions between the nanoparticles and the matrix are established at the molecular scale. This is consistent with the observed broadening of the signals of the low condensation groups in the nanocomposites, which can be explained by the larger chemical and structural diversity of environments caused by the zinc centers. In this respect, the Si–O–H groups present in the Q_2, Q_1 and Q_0 groups may be partially or totally substituted by Si–O–Zn bonds; such a substitution causes only a slight increment of chemical shift as can be evidenced from literature values reported for hemimorphite (Q_1)[23] and from the present results for β-Zn_2SiO_4 (Q_0). On the other hand, the Q_4 and Q_3 groups have very similar fwhm values for both the nanocomposites and the silica matrix at each T_{treat} value. This indicates that they are far from the zinc centers and so are unaffected by the presence of metal ions.

For a deeper insight into the structural evolution of the nanocomposites with T_{treat}, other important observations should be considered.

The evolution of each Q_n% is not as regular with temperature, in comparison to silica samples. Particularly for $Zn_{34}500$, Q_4% exhibits a minimum (Fig. 6), though Q% should be expected to remain constant if ZnO was merely to act as a physical obstacle to silica condensation. The observed result indicates that reaction between ZnO and silica occurs upon heating which causes a depolymerization of the host matrix at the interface and progressive formation of low condensation groups. As a consequence of the increased formation of superficial Q_n groups, the internal sites become more accessible to the nanoparticles, as established by the drastic reduction in Q_4%.

A small fraction of the Q_1 and Q_0 groups form progressively in the nanocomposites with increasing temperature, while they are completely absent in the silica matrix. Their presence cannot be accounted for by a chemical dispersion of zinc ions in the silica matrix, in which case the greatest differences between nanocomposites and the silica matrix should be expected at $T_{treat} = 300$ °C, at which temperature only minor changes have been observed. This observation confirms the results of previous studies[24,25] which showed that when the metal ions are introduced in the starting solution in the form of inorganic salts, they do not participate directly in the sol–gel chemistry. This indirectly confirms the TEM observation of a separate phase of zinc oxide nanoparticles.

Conversely, the appearance of the Q_1 and Q_0 groups can be interpreted in terms of formation of a disordered phase of zinc silicate. This is also consistent with the XRD pattern of the $Zn_{34}700$ and $Zn_{17}700$ samples, which do not exhibit peaks attributable to a new emerging crystalline phase. In any case, the amount of such low condensation sites is very small ($\leqslant 5$%), indicating that only a small fraction of ZnO has reacted with silica, producing the silicate phase, presumably at the nanoparticle/matrix interface, while the majority of ZnO is still present in form of nanoparticles dispersed in the silica network.

The behaviour of the $ZnO–SiO_2$ system is very different from that observed for the previously investigated $Fe_2O_3–SiO_2$ nanocomposites,[6,7] for which both IR and NMR spectroscopy indicated that the host matrix structure was substantially unaltered by the presence of iron oxide nanoparticles. The different chemical properties of the metal oxides are the main reason for the observed behaviour. It cannot be ruled out, however, that some changes in the matrix structure at the interface with iron oxide nanoparticles may not be revealed owing to interaction of paramagnetic iron with a number of silicon atoms causing broadening of part of the NMR signal. Conversely, the presence of diamagnetic zinc ions in this work has made it possible to measure more reliable ^{29}Si NMR signals that contribute valuable information on the nanoparticle/matrix interface of the $ZnO–SiO_2$ system.

Acknowledgements

This work has been supported by MURST and CNR (Rome, Italy).

References

1 S. Komarneni, *J. Mater. Chem.*, 1992, **2**, 1219.
2 O. Clause, M. Kermarec, L. Bonneviot, F. Villain and M. Che, *J. Am. Chem. Soc.*, 1992, **114**, 4709.
3 M. Kermarec, J. Y. Carriat, P. Burattin, M. Che and A. Decarreau, *J. Phys. Chem.*, 1994, **98**, 12008.
4 C. R. F. Lund and J. A. Dumesic, *J. Phys. Chem.*, 1981, **85**, 3075.
5 C. Chanéac, E. Tronc and J. P. Jolivet, *J. Mater. Chem.*, 1996, **6**, 1905.
6 G. Concas, G. Ennas, D. Gatteschi, A. Musinu, G. Piccaluga,

C. Sangregorio, G. Spano, J. L. Stanger and D. Zedda, *Chem. Mater.*, 1998, **10**, 495.
7 C. Cannas, D. Gatteschi, A. Musinu, G. Piccaluga and C. Sangregorio, *J. Phys. Chem. B*, 1998, **102**, 7721.
8 S. Bruni, F. Cariati, M. Casu, A. Lai, A. Musinu, G. Piccaluga and S. Solinas, *Nanostruct. Mater*., in press.
9 T. K. Gupta, *J. Am. Ceram. Soc.*, 1990, **73**, 1817.
10 Kang XueYa, Wang TianDiao, Han Yin, Tao MinDe and Tu MingJing, *Mater. Res. Bull.*, 1997, **32**, 1165 and references therein.
11 E. A. Meulenkamp, *J. Phys. Chem. B*, 1998, **102**, 5566.
12 S. Lu, L. Zhang and X. Yao, *Chin. Sci. Bull*., 1996, **41**, 1923.
13 L. Khouchaf, M. H. Tullier, M. Wark, J. J. Paillaud and M. Soulard, *J. Phys. IV*, 1997, **7**, C2.
14 Powder Diffraction File, Card No. 19–1479 (*International Center for Diffraction Data*, *Swarthmore*, *PA*).
15 Powder Diffraction File, Card No. 36–1451 (*International Center for Diffraction Data*, *Swarthmore*, *PA*).
16 E. Lippmaa, M. Magi, A. Samoson, G. Engelhardt and A. R. Grimmer, *J. Am. Chem. Soc.*, 1980, **102**, 4889.
17 F. Cesare Marincola, M. Casu, A. Lai, A. Musinu and G. Piccaluga, *J. Non-Cryst. Solids*, 1998, **232**, 329.
18 G. Engelard and D. Michel, *High Resolution Solid State NMR of Silicates and Zeolites*, J. Wiley & Sons, New York, 1987, ch. 5, p. 159.
19 K. L. Walter, A. Wokaum, B. E. Handy and A. Baiker, *J. Non-Cryst. Solids*, 1991, **134**, 47.
20 H. F. Taylor, *J. Am. Chem. Soc*., 1962, **47**, 932.
21 G. E. Maciel, *J. Am. Chem. Soc*., 1980, **102**, 7607.
22 D. W. Syndorf and G. E. Maciel, *J. Phys. Chem.*, 1982, **86**, 5208.
23 M. Magi, E. Lippmaa, A. Samoson, G. Engelhardt and A. R. Grimmer, *J. Phys. Chem.*, 1984, **88**, 1518.
24 S. Roy and D. Chakravorty, *J. Mater. Res.*, 1994, **9**, 2314.
25 G. Pantano, R. K. Brow and L. A. Carman, in *Sol–Gel Technology*, ed. L. C. Klein, Noyes Publications, NJ, 1990, vol. 6, p. 110.

Paper 9/01001G